Positron depth profiling of the structural and electronic structure transformations of hydrogenated Mg-based thin films

S. W. H. Eijt,[1,a)] R. Kind,[1] S. Singh,[1] H. Schut,[1] W. J. Legerstee,[1] R. W. A. Hendrikx,[2] V. L. Svetchnikov,[3] R. J. Westerwaal,[4] and B. Dam[4]
[1]*Department of Radiation, Radionuclides and Reactors, Faculty of Applied Sciences, Delft University of Technology, NL-2629 JB Delft, The Netherlands*
[2]*Department of Materials Science & Engineering, Faculty of Mechanical, Maritime and Materials Engineering, Delft University of Technology, NL-2628 CD Delft, The Netherlands*
[3]*Kavli Institute of Nanoscience, Faculty of Applied Sciences, Delft University of Technology, NL-2628 CJ Delft, The Netherlands*
[4]*Condensed Matter Physics, Vrije Universiteit, NL-1081 HV Amsterdam, The Netherlands*

(Received 31 October 2008; accepted 19 December 2008; published online 24 February 2009)

We report positron depth-profiling studies on the hydrogen sorption behavior and phase evolution of Mg-based thin films. We show that the main changes in the depth profiles resulting from the hydrogenation to the respective metal hydrides are related to a clear broadening in the observed electron momentum densities in both Mg and Mg_2Ni films. This shows that positron annihilation methods are capable of monitoring these metal-to-insulator transitions, which form the basis for important applications of these types of films in switchable mirror devices and hydrogen sensors in a depth-sensitive manner. Besides, some of the positrons trap at the boundaries of columnar grains in the otherwise nearly vacancy-free Mg films. The combination of positron annihilation and x-ray diffraction further shows that hydrogen loading at elevated temperatures, in the range of 480–600 K, leads to a clear Pd–Mg alloy formation of the Pd catalyst cap layer. At the highest temperatures, the hydrogenation induces a partial delamination of the ~5 nm thin capping layer, as sensitively monitored by positron depth profiling of the fraction of ortho-positronium formed at interface with the cap layer. The delamination effectively blocks the hydrogen cycling. In Mg–Si bilayers, we investigated the reactivity upon hydrogen loading and heat treatments near 480 K, which shows that Mg_2Si formation is fast relative to MgH_2. The combination of positron depth profiling and transmission electron microscopy shows that hydrogenation promotes a complete conversion to Mg_2Si for this destabilized metal hydride system, while a partially unreacted, Mg-rich amorphous prelayer remains on top of Mg_2Si after a single heat treatment in an inert gas environment. Thin film studies indicate that the difficulty of rehydrogenation of Mg_2Si is not primarily the result from slow hydrogen dissociation at surfaces, but is likely hindered by the presence of a barrier for removal of Mg from the readily formed Mg_2Si. © *2009 American Institute of Physics*.
[DOI: 10.1063/1.3075762]

I. INTRODUCTION

In view of the importance of the development of sustainable energy systems, hydrogen as an energy carrier is one of the prime candidates for enabling future clean energy supplies.[1,2] In this context, intensive current research focuses on the development of suitable materials for light-weight storage of hydrogen. Metal hydrides are promising for the compact storage of hydrogen[3,4] needed in the automotive industry. Many metals and metal alloys are available which absorb hydrogen,[4] involving the formation of metal hydrides such as MgH_2, $NaAlH_4$ and Mg_2NiH_4, creating a large research field to investigate and tailor their hydrogen sorption properties. In the framework of a hydrogen-based economy, Mg-based metal hydrides further show large promise for use in applications such as thin film hydrogen sensors,[5] hydrogen switchable mirror devices,[6,7] and Ni-metal hydride rechargeable batteries.[8] For example, Mg_2Ni serves as the active layer in switchable mirror devices[7] and is promising for tuning the transmission of energy-saving windows, with high reflectivity in both the visible and infrared regions of the solar spectrum. Further, the achievable fast switching times enable its use as a hydrogen sensor.[5]

The development of probes to characterize *in situ* the evolution of metal hydride thin films during hydrogen cycling is therefore important. In this perspective, positron annihilation methods,[9,10] applied widely in the field of thin film microelectronic active layers,[9] are promising owing to their depth-profiling capabilities typically in the submicrometer range, and their sensitivity to the local electronic properties, the material phase, and the presence and type of vacancy-related defects. Previous thermal desorption and structural studies on Mg thin films[11] presented complementary positron depth-profiling data, which indicate that open-volume defects appear in the Pd cap layer after the first decomposition of the MgD_2 film, without affecting the catalytic activity of the cap layer. Further, the depth profiles presented in Ref. 11 showed that relatively large changes in the positron Doppler broadening *S*-parameter of the metal hydride layer occurred

a)Electronic mail: s.w.h.eijt@tudelft.nl.

with hydrogen cycling at moderate temperatures up to 390 K.

In the present study, we clarify in detail the nature of the changes in positron Doppler broadening obtained on these types of metal hydride films and show their close relationship with the metal-insulator transition induced by the hydrogenation. In addition, we investigate the transformation of the catalyst cap layer at higher hydrogen cycling temperatures using positron depth profiling and x-ray diffraction (XRD). Metal-to-insulator transitions are at the basis of the functionality of switchable mirrors and thin film hydrogen sensor devices, and we show in this study that positron methods may retrieve the corresponding changes in local electronic properties. Further, the use of a catalyst capping layer is often crucial for dissociation of hydrogen molecules at the outer surface of thin film devices based on Mg alloys and compounds such as Mg_2Ni.[5,12] Monitoring their hydrogen sorption behavior is therefore important to achieve long-term hydrogen cycling stability.

Our study addresses therefore both the issues of (i) depth-profiling investigation of the hydrogenation of thin metal films using positron annihilation and (ii) their electronic structure changes. Further, the large sensitivity of positron methods to determine the presence and type of vacancies provides a motivation to our combined structural (XRD and electron microscopy) and depth-profiling positron studies on these types of metal hydrides. Vacancies in both the metal and hydrogen sublattices of metal hydrides may play an important role in promoting hydrogen diffusion and the hydrogen sorption in metal hydrides and their composites.

In Sec. III, we discuss the evolution of positron depth profiles upon hydrogenation of Mg and Mg_2Ni thin films and show that the major changes are related to the largely modified electron states resulting from the metal-to-insular transition. Subsequently, in Sec. IV, the phase transformation of the catalyst capping layer, involving alloying of Pd and Mg, and the subsequent initial stages of delamination of the thin Pd–Mg cap layer as a function of the temperature of hydrogen loading are sensitively monitored using positron annihilation methods. In Sec. V, we investigate the layer-resolved solid-state reactions in Mg–Si bilayers, motivated by the better thermodynamic properties of MgH_2 by destabilization through addition of silicon. The modified hydrogenation reaction $(1/2)Mg_2Si+H_2 \rightarrow MgH_2+(1/2)Si$ leads to a significantly reduced hydrogenation enthalpy of $\Delta H=-36.4$ kJ/mole H_2, and a predicted operation temperature just above room temperature.[13] In previous studies it was found that rehydrogenation of Mg_2Si is difficult, and was only successful so far during ball milling under 2.0 MPa hydrogen pressure near room temperature, leading to the appearance of small (<5 nm) MgH_2 nanoparticles.[14] We performed thin film studies on appropriate Mg–Si bilayer systems as an aid to clarify the (lack of) reactivity and to gain an insight on the local transformations associated with the solid-state reactions. In particular, we compare hydrogen loading of the films (at a hydrogenation pressure above equilibrium for bare Mg, but below the equilibrium pressure of Si-destabilized Mg at 480 K) with a corresponding bare temperature treatment in an inert noble gas environment.

II. EXPERIMENTAL

Mg films and Mg–Si bilayer films were deposited on glass substrates by dc magnetically confined plasma sputter deposition[12] using an argon plasma at a pressure in the range of 0.1–0.3 Pa, and Mg (99.9% pure) and Si wafers as sputter targets. Pd capping layers were subsequently deposited *in situ*. Hydrogen loading was carried out at a pressure of 1.0 MPa and at temperatures ranging from 480 to 500 K for 12 to 24 h. A homebuilt thermal desorption setup, HYDRA, was used for this purpose.[12] The Mg_2Ni films were deposited using magnetron deposition methods,[15,16] and some of the films were subsequently hydrogenated *ex situ*. The Mg and Mg–Si films were characterized by XRD using a Bruker-AXS Type D5005 at the Cu $K\alpha_1$ wavelength. Cross-sectional transmission electron microscopy (TEM) was carried out on selected films using a Philips CM30T microscope at 300 kV. In addition, selected area electron diffraction (SAED) images were obtained on cross sections of the films using a beam spot size equivalent to about the thickness of the film.

The positron Doppler broadening of annihilation radiation (511 keV) was measured using positrons with a kinetic energy in the range of 0–25 keV. Momentum windows $|p|<(3.0\times10^{-3})m_oc$ and $(8.2\times10^{-3})m_oc<|p|<(23.4\times10^{-3})m_oc$ for *S* and *W*, respectively, were used.[9,10] The *S* parameter is a measure of annihilation with valence electrons, providing sensitivity to the electronic structure and the presence of vacancies, while *W* is a measure for positron annihilation with semicore electrons, providing chemical sensitivity to the positron trapping site. The *S*-parameter depth profiles were analyzed using the VEPFIT program, which solves the full positron implantation-diffusion problem for a system of layers and calculated $S(E)$ curves are fitted to the experimental data, with the *S*-parameter of the respective layer, its thickness and positron diffusion length for each layer with a given mass density as fit parameters. Mahkovian implantation profiles were assumed with an average implantation depth (in nm) according to $z\sim(36/\rho)E^n$, with the implantation energy *E* in keV, the empirical value for the exponent set at $n=1.62$, and the density ρ in g/cm^3.[10] For more detailed characterization, depth-selective two-dimensional angular correlation of annihilation radiation (2D-ACAR)[17] measurements were performed on a Mg thin film annealed in He, employing the intense variable energy positron beam POSH (Ref. 17) and a positron implantation energy of 5 keV.

III. HYDROGENATION-INDUCED ELECTRONIC STRUCTURE AND PHASE TRANSFORMATIONS OF MG AND MG_2NI FILMS

Figures 1(a) and 2(a) show representative positron depth profiles of the Doppler *S*-parameter for as-deposited and hydrogen loaded Mg and Mg_2Ni thin films, respectively. The three regions corresponding to the ~5 nm Pd capping layer, the Mg or Mg_2Ni metal hydride layer, and glass substrate are clearly resolved in the Doppler depth profiles shown in Figs. 1(a) and 2(a). Upon hydrogenation, large changes in the positron Doppler *S*-parameter associated with the formation of the metal hydride in the second layer are seen, while the

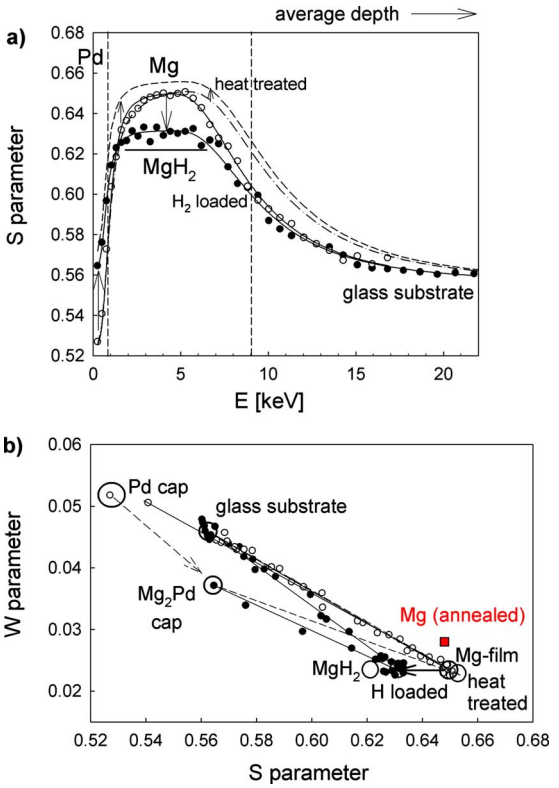

FIG. 1. (Color online) (a) Doppler *S*-parameter depth profiles for as-deposited Pd-capped Mg films and subsequent hydrogen loading (open and filled circles) or heat treatment under an inert He environment (dash-dotted and dashed lines). (b) Corresponding *S*-*W* diagram, with positron implantation energy *E* as the running parameter.

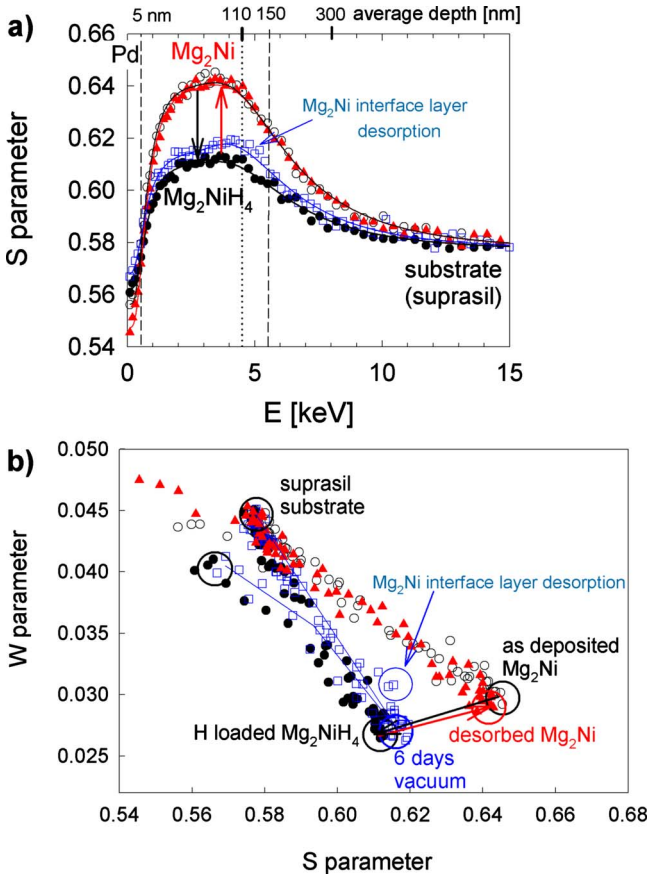

FIG. 2. (Color online) (a) Doppler *S*-parameter depth profiles for Pd-capped Mg_2Ni films. (i) As-deposited film (hollow circles); (ii) hydrogen loaded film (filled circles); (iii) partially desorbed film after 6 days in vacuum (hollow squares); (iv) desorbed film (filled triangles). (b) Corresponding *S*-*W* diagram; the running parameter is the positron implantation energy *E*.

glass substrate, as expected, is inert against hydrogen loading. The solid lines in Figs. 1(a) and 2(a) represent the VEPFIT analysis of the Doppler depth profiles.

In Figs. 1(b) and 2(b) the corresponding *S*-*W* diagrams are shown, which is a convenient way to examine the phase and defect evolution of the different layers.[9] Defect-free bulk materials are characterized by a specific well-determined characteristic *S*-*W* point, and relative changes with respect to this bulk *S*-*W* point can be utilized to determine the presence and type of defects detected in a positron study. The characteristic *S*-*W* point for well-annealed bulk crystalline Mg is included in Fig. 1(b), as determined in one of our recent previous studies[18] using the same experimental setup and settings. Clearly, the *S*-*W* point for the as-deposited Mg film is close to that of bulk annealed Mg, showing that positron trapping and positronium formation in large vacancy clusters (nanovoids are stable at room temperature) is absent. This would result, namely, in substantially higher *S*-parameter values up to ~0.72, as demonstrated in our additional experiments involving ion implantation of some of the Mg samples studied previously in Ref. 18 at a dose of 5×10^{16} He^+ ions/cm^2 using an implantation energy of 140 keV. The very high *S*-parameter ~0.72, observed already for the as-implanted samples and which remains high after thermal annealing at 725 K for 50 min, is related to the presence of nanovoids in Mg formed by clustering of the abundant, highly mobile vacancies created by the ion implantation process. The small but distinct difference in Fig. 1(b) of the *S*-*W* point of the as-deposited Mg layer relative to that of bulk Mg indicates nevertheless that some defect trapping occurs. The increase in *S*-parameter of +0.45% is somewhat smaller than the +0.6% increase reported by Segers *et al.*[19] for positron trapping in thermally induced monovacancies in Mg at elevated temperatures of about 900 K, indicating that the positron trapping is not saturated here even when monovacancies would be present in the Mg layer. A substantial fraction of the positrons in fact annihilate in a bulklike Mg environment. This can be understood since positron studies by Hautojaervi *et al.*[20] and Segers *et al.*[19] using defect quenching and annealing of Mg samples demonstrated that Mg vacancies are highly mobile (the migration energy is ~0.5 eV), and a complete annealing of vacancies and small vacancy clusters occurs well below room temperature. Appreciable defect concentrations on the order of 10^{-6} or higher are reached only at temperatures above about 700 K in thermodynamic equilibrium,[19,20] and positron trapping [the positron trapping energy is ~0.34 eV (Ref. 21)] in these thermally generated vacancies was detected only at such high temperatures. At the lower temperatures used in our studies, vacancies and small vacancy clusters anneal out to very low equilibrium concentrations leading to negligible positron trapping. Some of the positrons, however, may trap at the column boundaries observed for these types of sputter deposited films[12] consisting of columns with lateral spacing of

~100–150 nm in width. Grain boundaries within the columns of the Mg layers, in contrast, would be mobile in the presence of vacancies and would effectively absorb monovacancies in Mg at the relevant temperatures of the present experiments.[22] The positrons, therefore, detect a bulklike Mg local environment inside the columns, while some of the positrons after diffusion in a column may trap at vacancy clusters present at the boundaries of the columns.

Figure 1 shows that, upon subsequent loading of Mg films with hydrogen, the *S*-parameter decreases substantially with the transformation to the rutile MgH_2 phase. It is further noteworthy that the *W*-parameter stays nearly constant upon hydrogenation. For low-temperature hydrogen loading and desorption it was found that these *S*-*W* values return to their original values. The large reduction in Doppler *S*-parameter upon hydrogen loading of the Mg and Mg_2Ni layers turns out to be related primarily to the metal-to-insulator electronic structure transition accompanying the hydrogenation-induced phase transformation. The electronic state of valence electrons will change with the different nature of atomic binding in the two phases, as seen in the depth profiles by the large change in *S* and nearly constant value for *W* for the Mg film ($\Delta S/S=-3\%$, $\Delta W/W=0\%$) as apparent in Fig. 1(b). XRD showed that this particular film was hydrogenated partially, attaining a MgH_2 phase fraction of ~63% (~5 wt % hydrogen loading). The estimated change in Doppler *S*-parameter for the complete transformation of Mg to MgH_2 is therefore $\Delta S/S\sim-4.5\%$, i.e., close to the reduction of ~5% reported by Checchetto *et al.*[11] The reduction in the *S*-parameter stems from a clear broadening in the valence part of the electron momentum density with formation of the metal hydride, as observed in a Compton scattering study on Mg and MgH_2 powders by Garreau and Loupias.[23] The reduction is therefore primarily related to the change in valence electron momentum distributions (EMDs) of the bulk metal and metal hydride systems, as supported by the calculated momentum distributions of valence electrons in Mg and MgH_2 shown in Fig. 3(a).[24,25] Brancewicz *et al.*[24] showed that the nearly isotropic valence EMD of Mg can be excellently approximated by an inverted parabola with a Fermi momentum cutoff at $p_F\sim(5.3\times10^{-3})m_oc$ characteristic of a free-electron system.[24,26] The broadening results qualitatively from the more localized electron wave functions near the hydrogen positions. In particular, Yu and Lam[27] found that the Mg–H bonds in MgH_2 are primarily ionic, and not covalent, in character, with about 0.6 electron per H atom located at the H sites and about 19% of the valence band charges located interstitially. The resulting broadening in EMD, clearly visible from the calculations, is in a quite good agreement with the results from the Compton scattering study by Garreau.[23] We calculated that the expected fraction of valence electrons in the experimental momentum interval of $|p|<(3.0\times10^{-3})m_oc$ used in our Doppler study is about 7% lower for MgH_2 relative to Mg, using the theoretical momentum distributions convoluted with the resolution of $(2.9\times10^{-3})m_oc$ of the Doppler broadening measurements. This is close to the decrease of about 4.5% seen in positron experiments. The remaining difference can be related to the details of the spatial overlap of the positron

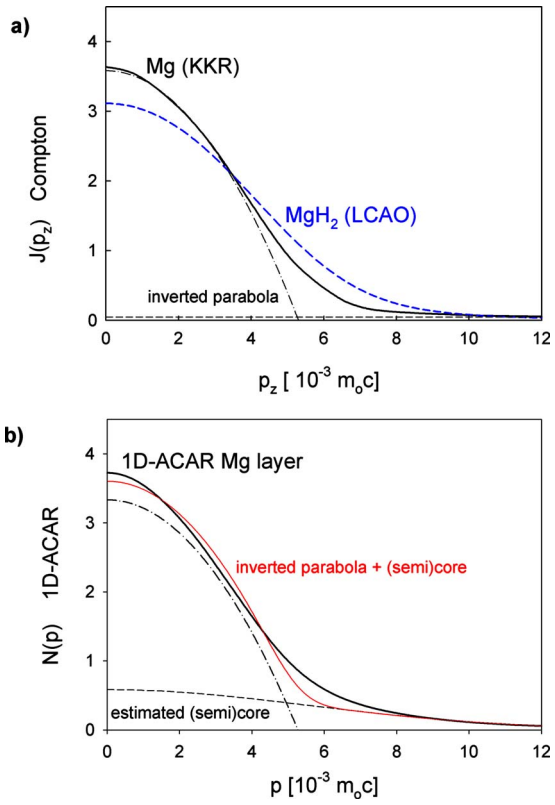

FIG. 3. (Color online) (a) Theoretical valence EMDs of Mg (Ref. 24, black full line) and MgH_2 (Ref. 25, blue dashed line) projected on the p_z-axis and convoluted with the experimental Compton scattering resolution with a full width at half maximum (FWHM) of $(2.9\times10^{-3})m_oc$. (b) 1D-ACAR of an as-deposited Mg film (sample 1a) obtained at a positron implantation energy of 5 keV (thick solid line). The (red) thin line shows comparison with the free-electron contribution (inverted parabola, dash-dotted line) with a Fermi momentum of $p_F=(5.3\times10^{-3})m_oc$ convoluted with the experimental resolution with a FWHM of $(1.4\times10^{-3})m_oc$ plus the estimated (semi-)core contribution (dashed line).

wave function with the valence electron orbitals, which was not included in these calculations, or, more likely as we will show below, to positron trapping in small vacancy clusters at the boundaries of columns in the Mg films. Positron trapping in hydrogen vacancies in the MgH_2 cannot strictly be excluded at this point, although the hydrogen vacancy formation energy for MgH_2 is relatively high, and appreciable vacancy concentrations in MgH_2 are therefore not expected in the temperature interval considered in this study.

Further insight was obtained by an additional study of an as-deposited Mg layer, which was subsequently heated at 480 K in an inert He environment, leading to a further increase in the *S*-parameter of the Mg layer, and the more pronounced shift of about +1.4% relative to well-annealed bulk Mg [Figs. 1(a) and 1(b)]. A high-resolution electron-positron momentum distribution was obtained on this sample using the positron 2D-ACAR method. The 2D-ACAR distribution at 5 keV was nearly isotropic, reflecting the almost isotropic valence band electronic structure of hcp Mg.[24] Figure 3(b) shows the extracted 1D-ACAR momentum distribution. While the Compton profiles reported in Ref. 24 and the corresponding calculated Compton profile of Fig. 3(a) can be described very well by an inverted parabola with Fermi momentum of $(5.3\times10^{-3})m_oc$ and taking the experimental res-

olution into account, the 1D-ACAR distribution shows clear deviations from such a free-electron-like component [Fig. 3(b)], in particular its center part is distinctly sharper. This shows that positron trapping in open-volume defects occurs, identified above as vacancy clusters located at the column boundaries, with a size larger than a monovacancy but much smaller than nanovoids. The overall momentum extension of the 1D-ACAR distribution nevertheless remains close to that of bulk Mg, and is distinctly sharper than that of MgH_2, showing that the observed large reduction in positron *S*-parameter upon hydrogenation is primarily related to the changes in electron momentum density resulting from the transformation from the metallic Mg to the insulator MgH_2.

Depth profiles [Fig. 2(a)] of the Doppler *S*-parameter for Mg_2Ni films show very similar changes upon hydrogen loading and unloading, suggesting that these are also closely related to the metal-to-insulator transition. Mg_2Ni and Mg both have a metallic electronic structure with a free-electron-like behavior of conduction band electrons, while MgH_2 and Mg_2NiH_4 both show ionic bindings of Mg with either the hydrogen atoms or the NiH_4 units.[27–30] Quantitatively similar changes are observed for Mg_2Ni in the *S*-*W* diagram [Fig. 2(b)] with hydrogen loading and unloading ($\Delta S/S_0 \sim -4.5\%$, $\Delta W/W_0 \sim -6\%$). A clear change in the Doppler *W*-parameter is now observed, which results from the reduced overlap of the positron wave function with the semicore Ni(3*d*) orbitals upon hydrogen loading, due to increased annihilation of positrons with H(1*s*) electron orbitals. Figures 4(a) and 4(b) show the measured electron-positron momentum density distribution for the Mg_2Ni film using the coincidence Doppler broadening method (at linear and logarithmic intensity scales) for positron implantation energies of 2 and 4 keV, respectively, showing in more detail the relationship to the electronic structure properties. The central part of the Mg_2Ni momentum distribution, up to about $(9 \times 10^{-3})m_oc$, is dominated by the contribution of the valence band electrons, primarily originating from Mg(3*s*) valence electron orbitals. Beyond this momentum range, the spatially more localized (semi-)core electrons—in particular the Ni(3*d*) electrons—account for most of the intensity, as is shown schematically in Figs. 4(a) and 4(b). Hydrogen desorption of Mg_2NiH_4 films results in a return of the measured positron *S*- and *W*-parameters to their original values, indicating the reversibility of the chemical and structural transformations.

The *S*-*W* points for the top Pd-capping layer show in general a large irreversible change upon initial hydrogen loading when using elevated loading temperatures. This effect is similar in size for all studied Mg and Mg_2Ni samples and was found to depend primarily on the application of the heat treatment rather than on the hydrogen loading itself, as will be discussed in more detail in Sec. IV.

Figures 2(a) and 2(b) further show that the interface layer of Mg_2NiH_4 with the substrate evolves differently upon desorption of the layer than the top part of the Mg_2NiH_4 layer, reflecting the difference in microstructure as reported in Ref. 15 with the occurrence of pores resulting from the initial growth of the film at the substrate. Namely, the *S*-parameter increases stronger with desorption at room temperature in a vacuum in the corresponding range of positron implantation energies between ~4 keV and ~6 keV than at lower implantation energies. Further, the corresponding *S*-*W* diagram in Fig. 2(b) shows, for this depth range, a clear deviation from the straight line connecting the *S*-*W* point of the top part of the film with the substrate *S*-*W* cluster point, with higher values for the *S*-parameter. The porous character of the interface layer is already visible in the *S*-parameter depth profile of the as-prepared Mg_2Ni films and appears in the coincident Doppler momentum distribution in Figs. 4(a) and 4(b) at a positron implantation energy of 4 keV (probing the interface layer to the substrate), which is sharper than the momentum distribution obtained at 2 keV (probing the middle of the Mg_2Ni layer). The different structural properties and hydrogen sorption behavior of the interface are noteworthy and reflect the findings by Lohstroh *et al.*[31] that this microporous interface layer is clearly the preferred hydroge-

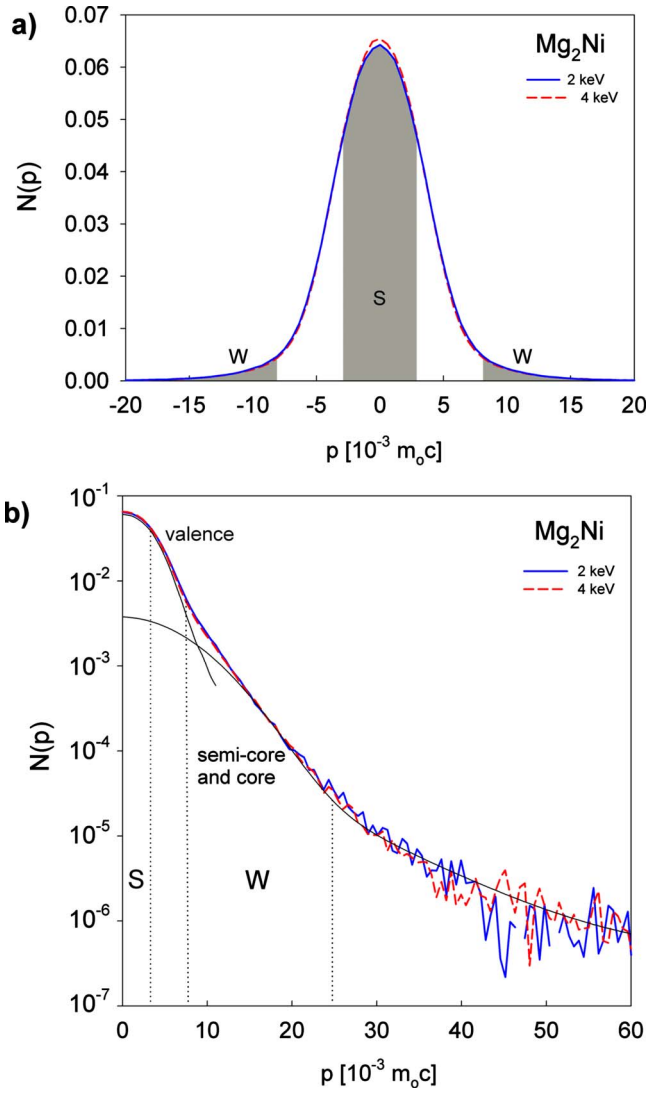

FIG. 4. (Color online) (a) Coincidence Doppler distribution of an as-deposited Mg_2Ni film at 2 keV (blue full line) and 4 keV (red dashed line), respectively. The shaded areas denote the intervals used to determine the *S*- and *W*- parameters. (b) Logarithmic representation of these coincidence Doppler distributions, showing the ranges of predominant contributions by valence electrons and semicore plus core electrons, respectively.

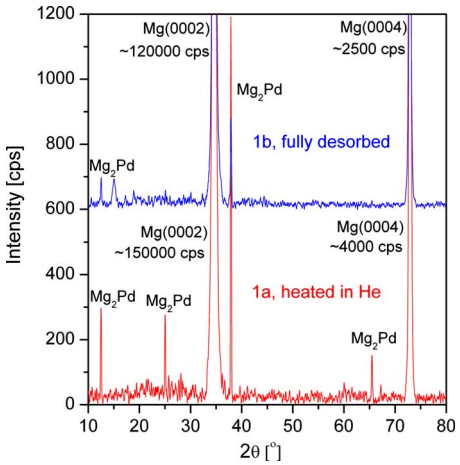

FIG. 5. (Color online) XRD patterns of Pd-capped Mg film (bottom) after heating in a He environment (red), (top) fully desorbed after loading with H_2, sample 1b (blue).

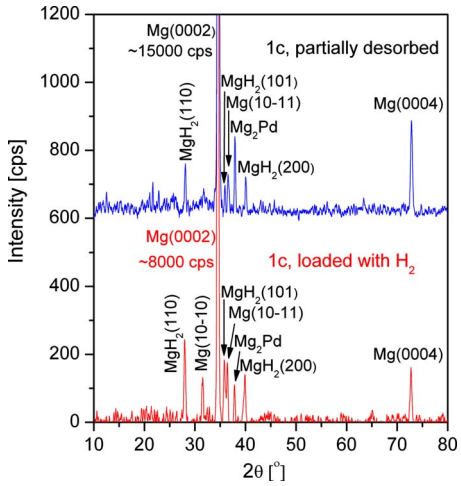

FIG. 6. (Color online) XRD patterns of Pd-capped Mg film (bottom) after loading with H_2, sample 1c (red), (top) after subsequent partial desorption, sample 1c (blue).

nation area, leading to the formation of an intermediate optical black-state upon hydrogenation of Mg_2Ni switchable mirrors.

IV. DEPTH-RESOLVED PD–MG ALLOYING AND INITIAL STAGES OF DELAMINATION OF PD CAP LAYERS

Subsequently, we investigated the effect of hydrogen cycling on the evolution of the Pd-capped Mg thin films using XRD and positron depth profiling. In particular, insight on the behavior of the Pd catalyst top layer and the adjacent Pd–Mg interface is desirable, since Pd diffusion and Mg–Pd alloy formation[32] and further delamination of the cap layer at elevated hydrogen loading temperatures[12] are known to diminish the catalytic activity upon continued hydrogen cycling. Our studies show that positron depth profiling is capable of providing such information even when using Pd-capping layers thinner than ~5 nm, and in addition gives an insight on the evolution of the phases of the layers consistent with complementary XRD data obtained on the films.

We exposed similarly prepared Pd-capped Mg films deposited on glass substrates to three different conditions in order to distinguish between (i) the effects of temperature treatment and hydrogen loading, and (ii) low temperature and high temperature hydrogen cycling. In Figs. 5 and 6 we show XRD patterns for the three different types of samples investigated: (1a) heating in an inert He environment at a temperature of 480 K; (1b) hydrogen loading at 480 K and desorption for temperatures below 498 K; and (1c) hydrogen loading at 500 K and desorption for temperatures up to 600 K. Hydrogen (or helium) pressures of 1.0 MPa were used for all samples, with exposure times of 24 h. Thermal desorption was performed at a temperature ramp rate of about 0.3 K/min.

The XRD pattern for sample (1a) shows a very intense Mg(0002) Bragg peak, which is also clearly present for the other samples. The XRD pattern for sample (1b) upon complete desorption after the first hydrogen loading treatment is very similar. The strongly preferred growth with the Mg *c*-axis plane parallel to the substrate surface is quite commonly observed on a variety of substrates, including, e.g., Al_2O_3 (Ref. 33) and Si(100).[12] We further note here that MgH_2 preferentially nucleates with the MgH_2(110) plane parallel to the Mg(0002) plane consistent with previous studies,[12,33,34] forming an interface with a fair lattice correspondence between the hcp Mg and rutile MgH_2 according to the structural model as described in Ref. 33.

Besides, Fig. 5 shows that four distinct additional Bragg peaks were detected in the XRD pattern, which fit the recently resolved Mg_2Pd structure.[35] Mg_2Pd diffraction peaks were also observed for the other samples both after hydrogen loading and after desorption, showing that a temperature treatment at a temperature of around 480 K alone is sufficient to lead to a high mobility of Pd and subsequent alloying of Pd and Mg in the top part of the films. The alloy formation is furthermore detected in the low energy (shallow depth) part of the positron depth profiles of Figs. 1, 7, and 8, visible in the strong shift in the *S*-parameter of the cap layer from about 0.525 to 0.563 in all these cases. This is seen even more explicitly in the corresponding *S*-*W* diagrams, showing that the change from Pd to the Mg_2Pd structure correlates with a strong shift in *S*-*W* cluster point for the Pd cap layer toward the Mg–Pd (Mg_2Pd) cluster point. This demonstrates that this change in top layer composition arises primarily from the temperature treatment, and associated enhanced Pd diffusion and Mg_2Pd alloy formation, and not from hydrogen loading itself.

The metal hydride layer also shows a distinct change with hydrogen loading and unloading. Figures 7 and 8 present the depth-resolved evolution of the samples 1c (high temperature hydrogen desorption) and 1b (low temperature hydrogen desorption). Doppler *S*-parameter depth profiles for an initially homogeneously hydrogen-loaded Mg-film are shown in Fig. 7(a) after two subsequent high temperature desorption runs for temperatures up to 573 and 600 K. The depth profiles are no longer flat in the range of 2–5 keV (Mg layer), but show a slow and gradual increase before saturating in the range of 6–8 keV. VEPFIT analysis[36] of the depth profiles are presented by the solid lines. The *S*-*W* diagram

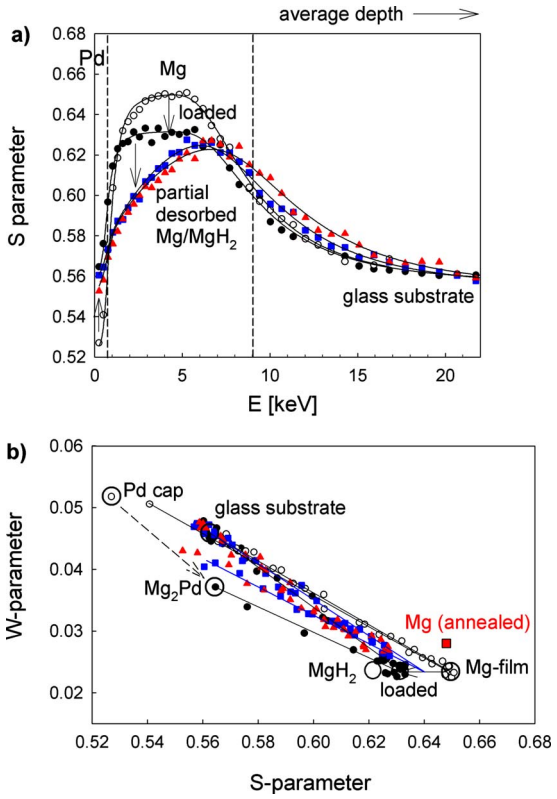

FIG. 7. (Color online) (a) Doppler *S*-parameter depth profiles for a Pd-capped Mg film, sample 1c. (i) As-deposited film (hollow circles); (ii) hydrogen loaded at 500 K (filled circles); (iii) first desorption up to 573 K (blue filled squares); (iv) second desorption up to 600 K (red filled triangles). (b) Corresponding *S*-*W* diagram.

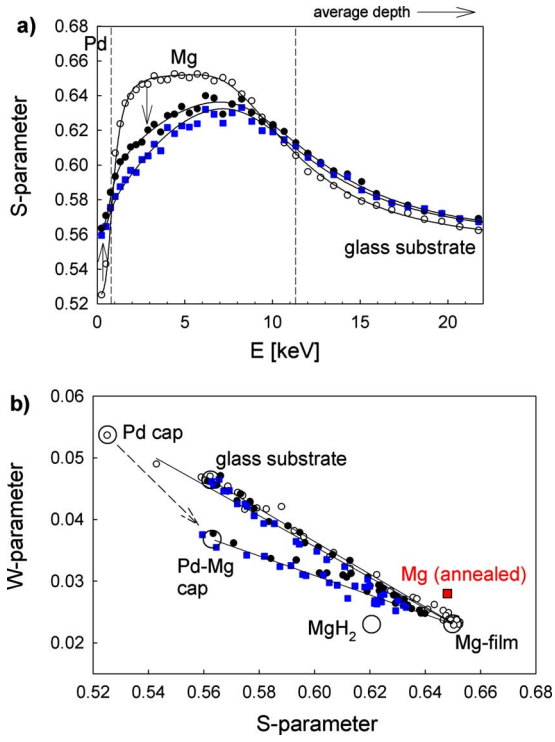

FIG. 8. (Color online) (a) Doppler *S*-parameter depth profiles for a Pd-capped Mg film, sample 1b. (i) As-deposited film (hollow circles); (ii) hydrogen loaded at 480 K (filled circles); (iii) desorption up to 498 K (blue filled squares). (b) Corresponding *S*-*W* diagram.

here shows a clear shift from the hydrogen loaded state to about halfway in between the points denoted loaded and Mg, showing that film (1c) is only partially desorbed, consistent with the observed changes in Bragg peak intensities (Fig. 6). We estimate, based on the intensities of the Mg(0002), MgH_2(110) and the presence of Mg(10–11) peaks in Fig. 6, that the sample was initially loaded to $63 \pm 5\%$ of a fully hydrogenated MgH_2 state. Subsequent desorption of the hydrided sample for temperatures up to 573 K leads to a clear increase in Mg peak intensities (Fig. 6), and a corresponding reduction in MgH_2 peaks, which, in contrast to sample (1b), however, do not completely disappear for the higher desorption temperatures of 573 and 600 K used, i.e., about $37 \pm 5\%$ of the layer still consists of MgH_2. In the interpretation of the Bragg peak intensities it is important to take into account that the MgH_2 domains are not entirely epitaxial with respect to the substrate,[12,37] but show a tilting relative to the surface normal as demonstrated from SAED imaging[12] while the Mg(0002) planes are accurately aligned, leading to relatively weak MgH_2 peaks in the diffraction pattern and broad rocking curves.[33,37]

Hydrogen loading and subsequent desorption at lower temperatures of 480 K and below 498 K (case 1b), respectively, in contrast leads to a complete hydrogen desorption as is evident from the corresponding XRD pattern in Fig. 5 obtained after the desorption step, which shows clear and strong Mg and Mg_2Pd Bragg peaks only, and from the corresponding *S*-*W* diagram of Fig. 8. The *S*-*W* diagram confirms that the metal hydride layer is nearly completely desorbed, since the data lie on a straight line connecting the characteristic *S*-*W* points for the Pd–Mg cap and an as-deposited Mg film. The data suggest that this occurred already after the initial hydrogen loading step, presumably during the sample transport in air, or due to desorption in the vacuum of the positron setup.

Insight on the different behavior of these similarly prepared Mg films desorbed up to different temperatures was obtained by monitoring the positron three-gamma decay. The three-gamma decay can be detected upon formation of ortho-positronium, a bound state of the positron with an electron, in the presence of open space of large enough volume such as at surfaces of metals, or in nanovoids with dimensions typically above ~ 1 nm. This method was employed recently as a very sensitive tool for monitoring nanopore networks in silica-based low-*k* dielectric films[38–40] and is based on detection of the three-gamma decay photons with energies below the 511 keV photon peak related with two-gamma pair annihilation. This is quantified by the positron *R*-value,[41] which can be converted to provide a direct measure of the formed ortho-positronium fraction.

The depth profiles for the o-Ps fraction for high temperature hydrogen loading and unloading (1c) are shown in Fig. 9(a). While the o-Ps formation probability was observed to be small for the other metal hydride films except for positrons implanted very close to the outer surface of the sample, the detected o-Ps fraction here is very high after the first desorption at high temperatures and decays only slowly with implantation depth. This strongly suggests that a significant part of the implanted positrons that diffuse back to the cap

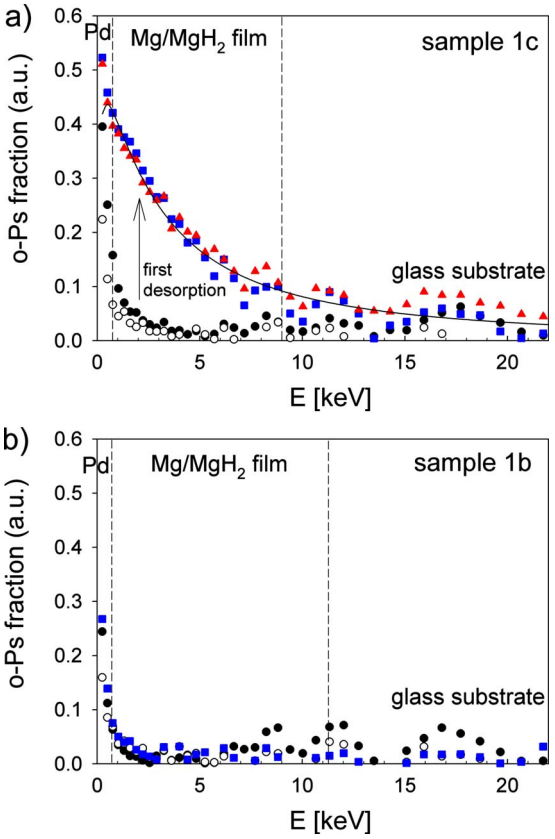

FIG. 9. (Color online) Ortho-positronium fraction $F_{\text{o-Ps}}(E)$ as a function of average implantation depth for sample 1c (top) and 1b (bottom). The high o-Ps formation and its slow decay with positron implantation energy for sample 1c indicate a pronounced positronium formation at the interface of the Mg layer with the capping layer.

layer are trapped at the interface between the metal/metal hydride layer and the cap layer, where they form o-Ps in appreciable quantities. VEPFIT analysis (full lines in Figs. 7 and 8) of the *S*-parameter depth profiles for samples 1c and 1b is consistent with an estimated positron diffusion length for defect-free Mg of $L_+=\sqrt{D_+\tau}\cong 192$ nm at room temperature. This value was deduced using the known positron lifetime of $\tau=219$ ps in bulk Mg and the diffusion constant $D_+=1.67$ cm s^{-1} estimated on the basis of *ab initio* calculations using the deformation potential theory[21,42,43] and experimental elastic constants of Mg as input parameters,[44] assuming that positron scattering to longitudinal acoustic phonons is dominant. The o-Ps fraction [Fig. 9(a)] was fitted by the equation $F_{\text{o-Ps}}(E)=F_{\text{o-Ps}}(0)/1+(E/E_0)^n$ according to diffusion-trapping theory,[41] using the same positron diffusion length of 192 nm with $L_+=(36/\rho)E_0^n$ and taking further the (higher) density of the thin Pd–Mg cap layer into account. The trapping is consistent with VEPFIT analysis of the *S*-parameter depth profiles, where a thin second layer was used to represent the strong trapping site (*S*-parameter $S=0.590$), while the fitted *S*-parameter of the Mg–MgH_2 metal hydride layer of $S=0.642$ is in between the Mg and MgH_2 values, consistent with the presence of both metal and metal hydride phases in the partially desorbed layer.

These observations clearly demonstrate that open volume is generated at the Mg_2Pd–Mg interface during desorption up to high temperatures, corresponding to a partial delamination of the capping layer from the metal hydride layer, as observed also for significantly thicker films upon hydrogen loading at temperatures typically above ~540 K.[12] The partial delamination of the cap layer leads to significantly higher temperatures needed to remove hydrogen from the buried Mg/MgH_2 surface, explaining that a part of the MgH_2 still remains in the film after hydrogen desorption up to a temperature of 600 K, i.e., lower than required for desorption from a bare Mg/MgH_2 surface. We attribute the delamination to a relatively weak adhesion of the Pd cap layer to the metal (hydride) layer, in combination with the relatively large lattice expansions upon hydrogenation of the Pd cap and Mg metal (hydride) layer, leading to correspondingly large stresses at the interface. Weak attachment of a Pd layer with a (glass) substrate was previously observed in studies on deposited Pd/Mg/Pd triple layers,[45] leading to complete detachment of the thickest triple layer films from the glass substrate at relatively low temperature (373 K) hydrogen loading, while the Pd–Mg attachment was found to sustain hydrogen loading at that temperature.

The depth profiles obtained for samples after hydrogen loading and desorption at lower temperatures of 480 K and below 498 K, respectively (Fig. 8) also reveal positron trapping at the Pd–Mg interface after desorption, indicating the presence of defects. Ps formation is, however, negligible in this case, excluding the formation of similar nanovoids and delamination. The trapping defects can be vacancy-type defects at the interface, e.g., related to the prestage of delamination involving breaking of bonds at the interface, to the diffusion of Pd, creating an intermixed interface area containing vacancies, or to the transformation of the top Pd–Mg layer into Mg_2Pd which may contain itself positron-trapping defects. Delamination itself does not yet occur at these temperatures, consistent with positron studies on Pd-capped Mg films at the still lower hydrogen sorption temperatures of around 373–390 K.[11] For completeness we note that the full VEPFIT analysis[36] of the positron Doppler curves in Figs. 1, 7, and 8 is consistent with this picture. More details can be found in the Appendix.

Summarizing the findings reported in this section, we conclude that Pd diffusion into the underlying Mg is significant already at temperatures of ~480 K employed in this study, leading to the formation of Mg_2Pd. Positron depth profiles and *S*-*W* diagrams for all samples show a corresponding large shift in the *S*-*W* parameters at low positron implantation depth from the Pd toward the Mg–Pd characteristic *S*-*W* point (Figs. 1, 7, and 8), revealing the cap layer transformation to Mg_2Pd. A very similar transformation was observed for the Mg_2Ni films after thermal desorption or high temperature hydrogen loading. Recent studies by Slack *et al.*[32] provide a clear indication for the loss of catalytic activity of Pd capping layers for Mg_2Ni films due to Pd diffusion. The use of an intermediate diffusion barrier (such as NbO_x) may aid to hinder the diffusion and limit the loss in the catalytic activity.[32] We further observed in the present positron depth-profiling study the partial delamination of the ~5 nm cap layer for hydrogen cycling in the higher temperature range around 573 K, leading to a loss of catalytic activity and incomplete desorption of hydrogen from the

metal hydride layer. Positron depth profiling therefore not only provides insight in the role and transformation of the catalyst used to promote hydrogen storage in metal hydrides, but may also aid in the development of metal hydride based devices by *in situ* monitoring of the catalyst and metal hydride layers, for example in the search of finding optimum layer sequences in metal hydride switchable mirrors.[32]

V. LAYER-RESOLVED MG_2SI FORMATION IN MG–SI BILAYER SYSTEMS

The presence of Si in the Mg–MgH_2 system is known to destabilize the metal hydride. In particular, the addition of Si to MgH_2 leads to modified hydrogen desorption and rehydrogenation reactions involving the more strongly bonded Mg_2Si instead of metallic Mg. A lower reaction enthalpy of metal hydride formation is thus obtained, following the rule that a more stable dehydrided phase leads to a corresponding lower stability of metal hydride. Vajo *et al.*[13] showed that the addition of Si indeed leads to higher equilibrium pressures and lower temperatures of hydrogen release. So far, however, it appeared difficult to reload the formed Mg_2Si (magnesium silicide), except during *in situ* ball milling under a 2.0 MPa hydrogen pressure resulting in the formation of MgH_2 particles with dimensions below about 5 nm.[14]

In order to better understand the interaction between Mg, MgH_2, and Si, we investigated the evolution of Mg–Si and Si–Mg bilayers on glass substrates created by subsequent sputter deposition of the respective species. In particular, we compared these types of bilayer systems upon hydrogen loading at 480 K using a 0.8 MPa hydrogen pressure and after a heat treatment at the same temperature in an inert He gas atmosphere, using XRD, positron depth profiling and electron microscopy for the analysis of the films. Mg and Si layers with thicknesses of ~400 nm and ~250 nm were used.

Figure 10(a) shows the positron Doppler *S*-parameter depth profiles obtained for the deposited Si–Mg and the Pd-capped Mg–Si bilayer systems. The order of the *S*-parameter values for Si, Mg, and the substrate ($S_{Mg} > S_{Si} > S_{substrate}$) enables an easy recognition of each individual layer in the depth profiles for the uncapped Si–Mg bilayer systems [Fig. 10(a)]. For the Mg–Si system on the other hand, the intermediate *S*-parameter value of Si obscures the visibility of the buried Si layer. The related *S*-*W* diagrams, shown in Fig. 10(b), unambiguously reveal the presence of the buried layer in both cases. The *S*-*W* diagram for Si–Mg bilayers enables one to identify the *S*-*W* point for the sputter deposited Si layers of ($S=1.02\ S_{c\text{-}Si}$, $W=0.85\ W_{c\text{-}Si}$). Comparison to previous studies on defects in Si layers shows that vacancy-related defects are present in the sputter deposited Si layer. The *S*-parameter is slightly smaller than the divacancy in c-Si ($S \sim 1.04\ S_{c\text{-}Si}$).[46] The *S*-*W* point is also very close to the *S*-*W* values of ($S=1.022\ S_{c\text{-}Si}$, $W=0.86\ W_{c\text{-}Si}$) and ($S=1.027\ S_{c\text{-}Si}$, $W=0.835\ W_{c\text{-}Si}$) reported in the study of a-Si:H films by Petkov *et al.*[47] for the D^o and D^- neutral and negatively charged defects, respectively. We can clearly rule out the presence of nanovoids in significant concentrations for these deposited Si films, as this would lead to radically different

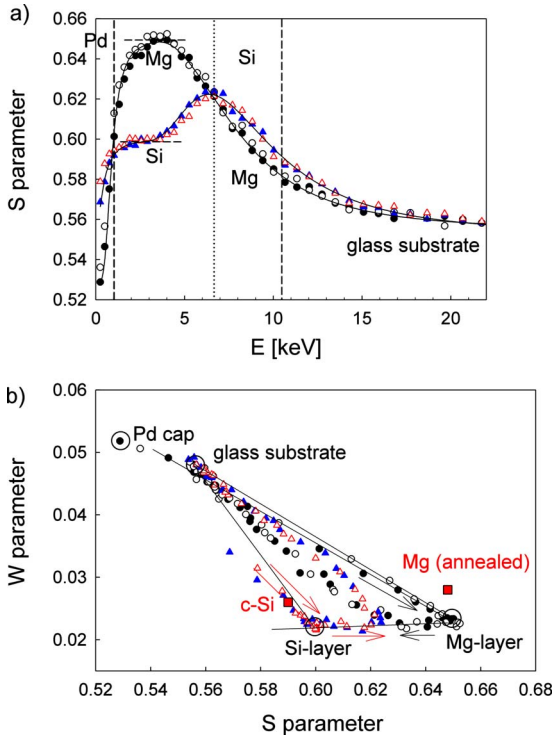

FIG. 10. (Color online) (a) Doppler *S*-parameter depth profiles for Pd-capped Mg–Si (filled and hollow circles) and uncapped Si–Mg (filled and hollow triangles) bilayer films. (b) Corresponding *S*-*W* diagram with positron implantation energy as running parameter.

S-*W* values approaching ($S=1.12\ S_{c\text{-}Si}$, $W=0.645\ W_{c\text{-}Si}$) as obtained for het-Si grown by HW-CVD using a H_2 and SiH_4 gas mixture.[48] These latter values are caused by the formation of Ps in the nanovoids. Clearly, both the sputter deposited Mg and Si layers are therefore dense.

The Mg–Si samples, capped *in situ* in the deposition process by a ~5 nm Pd layer, were subsequently loaded under an 0.8 MPa hydrogen atmosphere at 480 K for 24 h, respectively heated under an inert He atmosphere at 480 K for 24 h. The resulting positron Doppler depth profiles and *S*-*W* diagrams are given in Fig. 11. In both cases, XRD demonstrated that Mg_2Si is formed from the solid-state reaction of Mg and Si, with the preferred (111) orientation perpendicular to the sample surface, as shown in the diffraction patterns of Fig. 12 with the relatively strong $Mg_2Si(111)$ Bragg peak. A clear $Mg_2Si(111)$ texture was also reported in studies by Vantomme and Mahan,[49,50] who explored the formation of Mg_2Si films by codeposition of Mg and Si at substrate temperatures in the range between 473 and 873 K. No other crystalline phases besides Mg_2Si were detected here in the XRD patterns of Fig. 12, which are identical to within the experimental accuracy.

The positron depth profiles and *S*-*W* diagrams of Fig. 11 also clearly reveal the formation of the Mg_2Si phase, as apparent from the corresponding *S*-*W* cluster point at ($S=0.61$, $W=0.025$) present for both types of samples. The *S*-*W* value is reached for a positron implantation energy of ~6 keV, i.e., well in the reacted layer. Both the positron annihilation and XRD data show that heating (with or without the application of H_2) at 480 K is sufficient to lead to the formation of Mg_2Si. However, the positron depth profiles are qualitatively

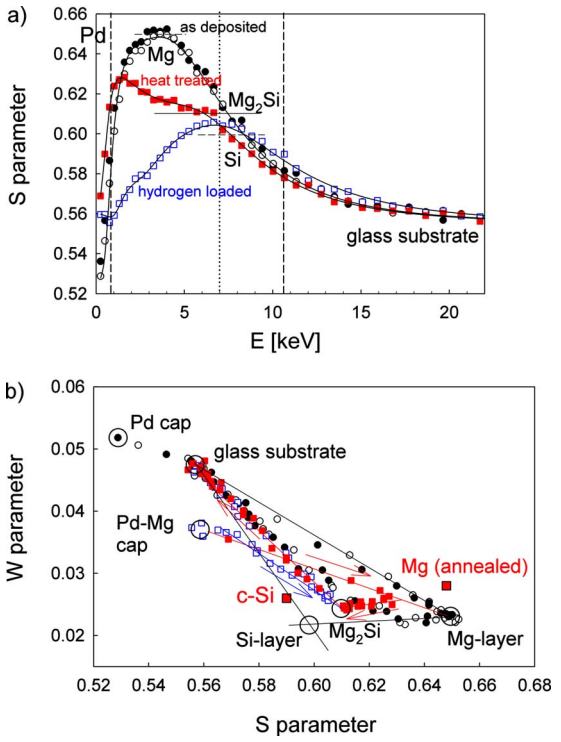

FIG. 11. (Color online) (a) Doppler *S*-parameter depth profiles for Pd-capped Mg–Si bilayer films; (i) as-deposited (filled and hollow circles), and after (ii) heating at 480 K in He, sample 2a (filled squares) and (iii) hydrogen loading at 480 K, sample 2b (hollow squares), respectively. (b) Corresponding *S*-*W* diagram.

different for the shallow subsurface layer region probed at positron implantation energies <5 keV. The *S*-*W* curve for the heat treated sample first moves from the Pd–Mg top layer in the direction of the Mg *S*-*W* cluster point suggesting the presence of a rather thin (amorphous) Mg-rich layer near the interface with the capping layer. Beyond an implantation energy of ~ 1.5 keV, positrons progressively see mainly the formed Mg_2Si layer, as evidenced by the subsequent sharp bending of the *S*-*W* curve toward the Mg_2Si *S*-*W* cluster point. The hydrogen loaded bilayer sample, in contrast, shows a change from the *S*-*W* point of the Pd–Mg cap layer directly toward that of Mg_2Si.

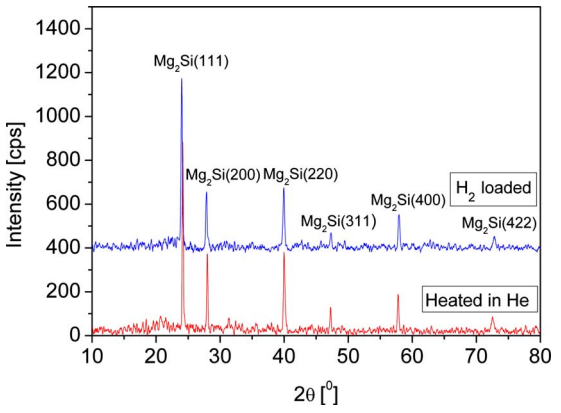

FIG. 12. (Color online) XRD patterns of Pd-capped Mg–Si bilayer films after hydrogen loading at 480 K, sample 2b (blue line, top), and heating at 480 K in He, sample 2a (red line, bottom), respectively, showing a clear Mg_2Si formation in both cases.

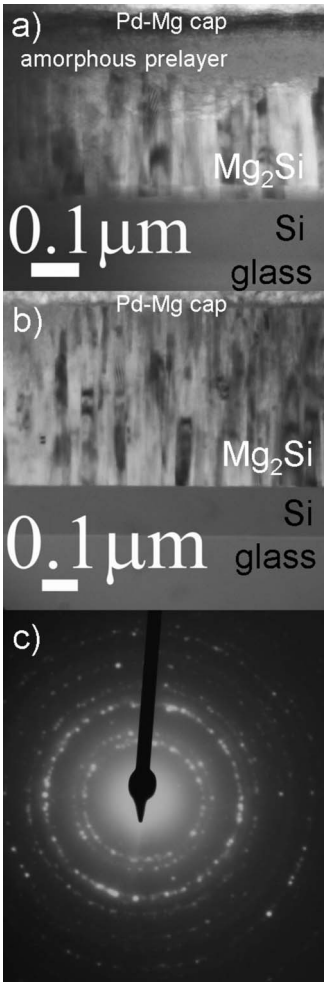

FIG. 13. Cross-sectional TEM images of Pd-capped Mg–Si bilayer films (a) after heating at 480 K in He (sample 2a) and (b) hydrogen loading at 480 K (sample 2b), respectively. Both samples show the presence of a Mg_2Si layer on top of a remaining thinner Si layer and glass substrate, as evidenced by (c) SAED patterns. In addition, the presence of an amorphous presumably Mg-rich prelayer is seen on various parts of the heat treated sample 2a, as shown in (a).

We attribute this difference in behavior for the hydrogenated sample to an alternative transformation of the layers to Mg_2Si during hydrogenation and initial formation of MgH_2 in the top part of the Mg layer. At this stage, Mg_2Si formation at the Mg–Si interface will occur simultaneously, which will be even accelerated by the significant heat release and local temperature rise caused by the hydrogenation of the prelayer to MgH_2 having a high enthalpy of formation. As soon as the zone with the reaction product Mg_2Si is in contact with the MgH_2 layer, destabilization will be effective, and the applied hydrogen pressure of 0.8 MPa will no longer be sufficient at the high temperature of the experiment to hinder complete hydrogen desorption of the MgH_2 prelayer, and a full transformation to Mg_2Si will then finally be reached.

We performed subsequent electron microscopy studies (see Fig. 13) which support this picture for the evolution of the layers schematically presented in Fig. 14. Figure 13 shows TEM images obtained for both types of samples and a representative SAED pattern. Clearly, in both cases a double layer of Mg_2Si, showing a columnar structure similar to Mg

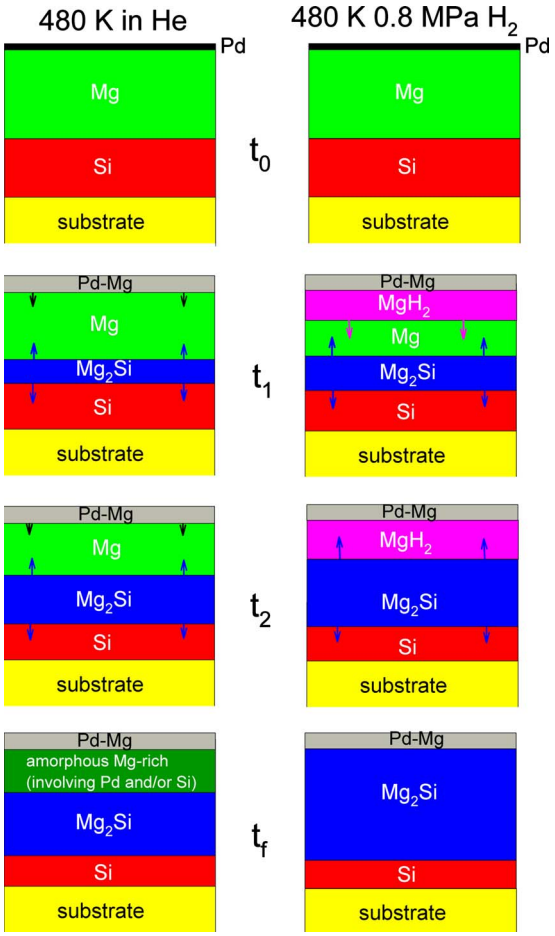

FIG. 14. (Color online) Schematic drawing of the proposed evolution of Pd-capped Mg–Si bilayers on a glass substrate upon prolonged (i) heating at 480 K in an inert He gas environment or (ii) hydrogen loading at 480 K at a pressure of 0.8 MPa. The hydrogen loading leads to a higher local temperature and faster transformation to Mg_2Si, and inhibits the formation of an amorphous Mg–Pd or Mg–Si prelayer. The initially formed MgH_2 releases all hydrogen when contact with Mg_2Si is reached.

films deposited at moderate temperatures,[12] on top of a thin and homogeneous Si layer is observed. The latter layer remains unreacted because of the nonstoichiometric ratio $Mg:Si<2:1$ for the Mg and Si layer thicknesses applied for these samples. In addition, for the heat treated sample, TEM images clearly reveal the presence of an amorphous layer on top of the Mg_2Si layer, which has a slowly varying thickness between 0 and ~200 nm across the sample area. This amorphous layer is not present in the hydrogenated sample and is consistent with the clear difference in the positron depth profiles at shallow depths below the outer surface of the samples. Most probably, the layer consists of a partially unreacted amorphous Mg or Mg-rich compound not detected in XRD, but which is clearly visible in the positron depth profile and *S-W* diagram of Fig. 11 (filled squares). Both magnesium-rich Mg–Pd alloys as well as silicon-rich and magnesium-rich Mg–Si alloys may form amorphous layers in sputtered deposited films.[51,52]

At this point it is interesting to compare to results of earlier studies. In our previous study,[12] Mg films which were deposited on Si wafers could be easily loaded by hydrogen and unloaded without significant Mg_2Si formation in the temperature range ~475 K–520 K, although at a high temperature of ~670 K silicide formation at the interface with the Si wafer was observed. There are clear differences between the use of Si wafers and the *in situ* deposited bilayer films, however. In particular, the latter have a fresh, fairly oxygen-free Mg‖Si interface, while Si wafers rapidly oxidize in the near-surface layer upon exposure to air. Such a barrier is known to act as a diffusion barrier for Mg, preventing silicide formation in this type of silicide compound.[53] Furthermore, the deposited bilayers likely are separated by a more corrugated Mg‖Si interface than in case of the flat wafer substrate. Finally, the deposited Si layer contains vacancy defects as detected in the present positron experiments, leading to higher Mg mobility. These factors, in particular the absence of an oxide diffusion barrier, will clearly promote the silicide formation reaction rates. Previous Kirkendahl effect studies using Xe tracer atoms and Rutherford backscattering show that Mg from 400 nm Mg layers deposited *in situ* on top of HF treated Si wafer substrates is highly mobile and moves into the Si layers to react to form Mg_2Si silicide.[53] Complete conversion to a 530 nm Mg_2Si layer was obtained at temperatures as low as 548 K in 70 min. Janega *et al.*[54] obtained a complete transformation to a polycrystalline Mg_2Si layer upon annealing a similar bilayer system in a N_2 atmosphere at 573 K for 30 min.

The origin of the irreversibility of the formed Mg_2Si with subsequent hydrogenation, as observed in a number of studies, most likely is related to the difficulty of removal of Mg from the Mg_2Si from its local tetrahedral binding geometry surrounded by four neighboring Si atoms. While thermodynamically the rehydrogenation step is favored at sufficiently high hydrogen pressures above the equilibrium pressure, the presence of a reaction barrier may obstruct the formation of local MgH_2 nuclei. This could also provide an explanation to the observed (partial) reversibility under *in situ* ball milling conditions using a 2.0 MPa H_2 pressure, since ball milling of metal hydrides often leads to stabilization of nonequilibrium phases and may further aid to overcome reaction barriers. One of the other mentioned bottlenecks proposed in the literature, namely slow hydrogen dissociation at Mg_2Si surfaces, can be disregarded since hydrogen is readily present in its atomic form in the thin film studies. Clemens *et al.*[37] recently showed, in fact, that atomic hydrogen can easily permeate Pd-capped Mg_2Si layers to fully hydrogenate Mg films underneath. Recent *ab initio* calculations[55] moreover show that hydrogen may dissociate easily at particular oxygen-free surfaces such as the $Mg_2Si(-110)$ surface.

VI. CONCLUSIONS

The present positron depth-profiling studies on the hydrogenation of Mg and Mg_2Ni layers show in a direct manner that the metal-to-metal-hydride phase transformations lead to a clear broadening of the EMDs. This reflects the large change in the electronic structure for the hydrogenation induced metal-to-insulator transition, in which the nearly free-electron-like Mg or Mg_2Ni metal transforms into an ionic metal hydride with a clear band gap, forming the basis

for applications as hydrogen sensors and electrochromic windows. Deposited Mg films have very low concentrations of Mg vacancies as implanted positrons detect primarily a bulklike crystalline Mg local environment, related to annealing of vacancies and small vacancy clusters in Mg below room temperature. Further, a fraction of the positrons trap at open spaces at the boundaries of columns of the nanostructured films. Clearly, our studies show that positron methods have a large potential for innovative depth-profiling studies on metal hydride films and devices, in particular when extended to *in situ* hydrogen cycling experiments monitoring the layer-resolved electronic structure transformation and the evolution of metal and/or hydrogen vacancy-related defects.

Hydrogen loading and desorption of Mg films at increased temperatures leads to large Pd mobility and clear Mg_2Pd alloy formation (for $T \sim 480$ K), as evidenced by XRD and positron depth-profiling analysis. The initial stages of delamination of ultrathin Pd-based cap layers were clearly resolved by positron depth profiling. In particular, upon heat treatment up to 600 K, the occurrence of a pronounced orthopositronium formation revealed the formation of nanoscale open spaces at the interface. As a consequence, the catalytic activity of the cap layer is reduced, and part of the hydrogen remains in the metal hydride layer. This type of reduced catalytic activity is known to be responsible for the decreased performance upon cycling of Pd-capped hydrogen switchable mirrors and hydrogen sensors. This infers that positron depth profiling is a very useful method to monitor *in situ* these processes leading to degradation of metal hydride thin film devices in a layer-resolved manner and can aid in the search to finding better catalyst cap layers.

Finally, we monitored the solid-state reactions of Mg–Si bilayers upon hydrogen loading and heat treatment in an inert gas environment, both leading to relatively fast Mg_2Si formation. Positron depth profiling revealed the appearance of an amorphous Mg-rich prelayer for heating solely, consistent with *a posteriori* analysis using electron microscopy. Rehydrogenation of Mg_2Si is difficult, most likely related to the presence of a barrier against removal of Mg from the Mg_2Si layer, inhibiting the formation of MgH_2. This suggests that reversibility could only possibly be retrieved when using an appropriate catalyst to lower this barrier, combined with the use of very small particles.

ACKNOWLEDGMENTS

This work was financed within the Sustainable Hydrogen Programme of the Delft Institute for Sustainable Energy (DISE), Delft University of Technology.

APPENDIX: VEPFIT ANALYSIS

The three layers (cap layer, metal/metal hydride layer, and substrate) in Figs. 1, 7, and 8 were modeled by 3 layers plus two additional 2 layers bordering the metal (metal hydride) layer with the same S-parameter but with a short positron diffusion length of $L_+=3$ nm to prohibit positrons to escape from the layer, as would be the case for the solution of the implantation-diffusion problem offered by VEPFIT for a three-layer system. In this way, the effect of the stronger positron affinity[56] for Mg ($A_+=-6.18$ eV) relative to Pd ($A_+=-5.04$ eV) can be correctly incorporated, without sacrificing in the modeling the freedom to select a (large) positron diffusion length in the buried metal or metal hydride layer. The fits showed that the S-parameters are similar [$S=0.651$ for the 654 nm Mg layer of Fig. 7(a) and $S=0.658$ for the 852 nm Mg layer of Fig. 8(a)], at a fixed positron diffusion length at its theoretical value of $L_+=192$ nm. Upon hydrogen loading or heating at 480 K, in particular the S-parameter of the cap layer and surface trapped positrons are seen to increase from $S=0.488$ (bulk Pd) and $S=0.524$, respectively, to the higher values of $S=0.570$ and $S=0.563$, similar to the shift in the S-W diagrams. These effects are primarily responsible for the increase of S-parameter throughout the depth profile for the heat treated sample (Fig. 1). The hydrogen loaded sample, in contrast, shows a strong homogeneous decrease to a value of $S=0.632$, i.e., about 3% lower. Thus, provided that the density of the resulting film is known, for example estimated from crystallographic information using XRD, the layer expansion associated with the metal/metal hydride transformation can be detected indirectly from the positron depth profile. The XRD patterns of the film show Bragg peaks at positions consistent with the bulk crystal structure of each of the phases, and bulk densities can be assumed to be good approximations.[12] Assuming a density of the layer of 1.54 g/cm^3 for the 63% hydrogenated mixed Mg/MgH_2 film results in a fitted 818 nm expanded film. Interestingly, the analysis therefore, albeit indirectly, reveals the large increase in the effective layer thickness (volume) upon hydrogenation by about +28%, which is of the same size as the +21% volume expansion expected for a 63% hydrogenated Mg sample. The fitted layer thicknesses for the Mg films are somewhat larger than the estimates based on quartz crystal microbalance and DekTak profilometry measurements on similarly prepared Mg films. This may indicate that the positron implantation profile with average depth according to $z \sim (36/\rho)E^n$ may be better described for Mg and MgH_2 by an exponent n smaller than the empirical value of $n=1.62$ obtained as an average for a large set of materials.[56] This may also affect the exact value for the relative volume change deduced from our measurements.

[1] L. Schlapbach and A. Züttel, Nature (London) **414**, 353 (2001).
[2] M. S. Dresselhaus and I. L. Thomas, Nature (London) **414**, 332 (2001).
[3] J. Huot, in *Nanoclusters and Nanocrystals*, edited by H. S. Nalwa (American Science, Stevenson Ranch, CA, 2003), Chapter 2, p. 53.
[4] G. Sandrock, J. Alloys Compd. **293–295**, 877 (1999).
[5] M. Pasturel, M. Slaman, D. M. Borsa, H. Schreuders, B. Dam, W. Lohstroh, and A. Borgschulte, Appl. Phys. Lett. **89**, 021913 (2006).
[6] J. N. Huiberts, R. Griessen, J. H. Rector, R. J. Wijngaarden, J. P. Dekker, D. G. de Groot, and N. J. Koeman, Nature (London) **380**, 231 (1996).
[7] T. J. Richardson, J. L. Slack, R. D. Armitage, R. Kostecki, B. Farangis, and M. D. Rubin, Appl. Phys. Lett. **78**, 3047 (2001).
[8] P. Vermeulen, R. A. H. Niessen, and P. H. L. Notten, Electrochem. Commun. **8**, 27 (2006).
[9] *Positron Beams and their Applications*, edited by P. G. Coleman (World Scientific, Singapore, 2000).
[10] P. J. Schultz and K. G. Lynn, Rev. Mod. Phys. **60**, 701 (1988).
[11] R. Checchetto, N. Bazzanella, A. Miotello, R. S. Brusa, A. Zecca, and A. Mengucci, J. Appl. Phys. **95**, 1989 (2004).
[12] S. Singh, S. W. H. Eijt, M. W. Zandbergen, W. J. Legerstee, and V. L. Svetchnikov, J. Alloys Compd. **441**, 344 (2007).

[13]J. J. Vajo, F. Mertens, C. C. Ahn, R. C. Bowman, Jr., and B. Fultz, J. Phys. Chem. B **108**, 13977 (2004).
[14]R. Janot, F. Cuevas, M. Latroche, and A. Percheron-Guégan, Intermetallics **14**, 163 (2006).
[15]R. J. Westerwaal, A. Borgschulte, W. Lohstroh, B. Dam, B. Kooi, G. ten Brink, M. J. P. Hopstaken, and P. H. L. Notten, J. Alloys Compd. **416**, 2 (2006).
[16]R. J. Westerwaal, C. P. Broedersz, R. Gremaud, M. Slaman, A. Borgschulte, W. Lohstroh, K. G. Tschersich, H. P. Fleischhauer, B. Dam, and R. Griessen, Thin Solid Films **516**, 4351 (2008).
[17]S. W. H. Eijt, A. Veen, H. Schut, P. E. Mijnarends, A. B. Denison, B. Barbiellini, and A. Bansil, Nature Mater. **5**, 23 (2006).
[18]J. Dryzek, H. Schut, and E. Dryzek, Phys. Status Solidi C **4**, 3522 (2007).
[19]D. Segers, M. Dorikens, and L. Dorikens-Vanpraet, Solid State Commun. **36**, 943 (1980).
[20]P. Hautojärvi, J. Johanson, A. Vehanen, J. Yli-Kauppila, J. Hillairet, and P. Tzanétakis, Appl. Phys. A **27**, 49 (1982).
[21]I. Makkonen and M. J. Puska, Phys. Rev. B **76**, 054119 (2007).
[22]O. A. Lambri, M. Massot, W. Riehemann, E. J. Lucioni, F. Plazaola, and J. A. Garçia, Phys. Status Solidi A **204**, 1077 (2007).
[23]Y. Garreau and G. Loupias, Solid State Commun. **74**, 583 (1990).
[24]M. Brancewicz, H. Reniewicz, A. Andrejczuk, L. Dobrzyński, E. Żukowski, and S. Kaprzyk, Solid State Phenom. **112**, 123 (2006).
[25]J. Felsteiner, M. Heilper, I. Gertner, A. C. Tanner, R. Opher, and K.-F. Berggren, Phys. Rev. B **23**, 5156 (1981).
[26]M. Y. Chou and M. L. Cohen, Solid State Commun. **57**, 785 (1986).
[27]R. Yu and P. K. Lam, Phys. Rev. B **37**, 8730 (1988).
[28]G. N. García, J. P. Abriata, and J. O. Sofo, Phys. Rev. B **59**, 11746 (1999).
[29]W. R. Myers, L.-W. Wang, T. J. Richardson, and M. D. Rubin, J. Appl. Phys. **91**, 4879 (2002).
[30]V. L. Morruzi, J. F. Janak, and A. R. Williams, *Calculated Electronic Properties of Metals* (Pergamon, New York, 1978), p. 49.
[31]W. Lohstroh, R. J. Westerwaal, B. Noheda, S. Enache, I. A. M. E. Giebels, B. Dam, and R. Griessen, Phys. Rev. Lett. **93**, 197404 (2004).
[32]J. L. Slack, J. C. Locke, S.-W. Song, J. Ona, and T. J. Richardson, Sol. Energy Mater. Sol. Cells **90**, 485 (2006).
[33]R. Kelekar, H. Giffard, S. T. Kelly, and B. M. Clemens, J. Appl. Phys. **101**, 114311 (2007).
[34]M. W. Zandbergen, S. W. H. Eijt, W. J. Legerstee, H. Schut, and V. L. Svetchnikov, Mater. Res. Soc. Symp. Proc. **837**, N1.3, p. 3 (2005).
[35]J. P. A. Makongo, Yu. Prots, R. Niewa, U. Burkhardt, and G. Kreiner, Z. Kristallogr. - New Cryst. Struct. **220**, 291 (2005).
[36]A. van Veen, H. Schut, J. de Vries, R. A. Hakvoort, and M. R. IJpma, AIP Conf. Proc. **218**, 171 (1991).
[37]B. Clemens, "Thermodynamically Tuned Nanophase Materials for Reversible Hydrogen Storage," Stanford University MH Center of Excellence DoE Hydrogen Program Annual Progress Report, 2006 (http://www.hydrogenenergy.gov/pdfs/review06/stp_5_clemens.pdf), IV.A.4l, p. 343.
[38]M. P. Petkov, M. H. Weber, K. G. Lynn, K. P. Rodbell, and S. A. Cohen, J. Appl. Phys. **86**, 3104 (1999).
[39]A. van Veen, R. Escobar Galindo, H. Schut, S. W. H. Eijt, C. V. Falub, A. R. Balkenende, and F. K. de Theije, Mater. Sci. Eng., B **102**, 2 (2003).
[40]D. W. Gidley, H.-G. Peng, and R. S. Vallery, Annu. Rev. Mater. Res. **36**, 49 (2006).
[41]K. G. Lynn, in *Positron Solid-State Physics*, edited by W. Brandt and A. Dupasquier (North-Holland, Amsterdam, 1983), p. 609.
[42]O. V. Boev, M. J. Puska, and R. M. Nieminen, Phys. Rev. B **36**, 7786 (1987).
[43]M. J. Puska, P. Lanki, and R. M. Nieminen, J. Phys.: Condens. Matter **1**, 6081 (1989).
[44]A. R. Wazzan and L. B. Robinson, Phys. Rev. **155**, 586 (1967).
[45]K. Higuchi, K. Yamamoto, H. Kajioka, K. Toiyama, M. Honda, S. Orimo, and H. Fujii, J. Alloys Compd. **330–332**, 526 (2002).
[46]H. Schut, S. W. H. Eijt, C. D. Beling, K. Ho, and Y. Takamura, Mater. Sci. Eng., B **124–125**, 283 (2005).
[47]M. P. Petkov, T. Marek, P. Asoka-Kumar, K. G. Lynn, R. S. Crandall, and A. H. Mahan, Appl. Phys. Lett. **73**, 99 (1998).
[48]A. Rivera, "Hydrogen Interactions with Silicon-on-Insulator Materials," Ph.D. thesis, Delft University of Technology, 2003.
[49]A. Vantomme, J. E. Mahan, G. Langouche, J. P. Becker, M. Van Bael, K. Temst, and C. van Haesendonck, Appl. Phys. Lett. **70**, 1086 (1997).
[50]J. E. Mahan, A. Vantomme, G. Langouche, and J. P. Becker, Phys. Rev. B **54**, 16965 (1996).
[51]K. Yoshimura, S. Nakano, S. Uchinashi, S. Yamaura, H. Kimura, and A. Inoue, Meas. Sci. Technol. **18**, 3335 (2007).
[52]T. Serikawa, M. Henmi, T. Yamaguchi, H. Oginuma, and K. Kondoh, Surf. Coat. Technol. **200**, 4233 (2006).
[53]W. K. Chu, S. S. Lau, J. W. Mayer, and H. Müller, Thin Solid Films **25**, 393 (1975).
[54]P. L. Janega, J. McCaffrey, D. Landheer, M. Buchanan, M. Denhoff, and D. Mitchel, Appl. Phys. Lett. **53**, 2056 (1988).
[55]B. Dai, D. S. Sholl, and J. K. Johnson, J. Phys. Chem. C **111**, 6910 (2007).
[56]M. J. Puska and R. M. Nieminen, Rev. Mod. Phys. **66**, 841 (1994).